International Journal of Automotive Technology, Vol. ?, No. ?, pp. ?–?(year)

ONLINE MISALIGNMENT ESTIMATION OF STRAPDOWN NAVIGATION FOR LAND VEHICLE UNDER DYNAMIC CONDITION

Yoonjin Hwang[1)], Yongseop Jeong[2)], In So Kweon[3)] and Seibum Choi[1)*]

[1)]Department of Mechanical Engineering, KAIST, Daejeon 34141, Korea
[2)]The Robotics Program, KAIST, Daejeon 34141, Korea
[3)] School of Electrical Engineering, KAIST, Daejeon 34141, Korea

(*Received date ; Revised date ; Accepted date*) * Please leave blank

ABSTRACT–In recent times, localization and positioning techniques have rapidly developed with the increasing demand for unmanned vehicles. Most positioning systems for land vehicles based on GPS-IMU, use a non-holonomic constraint to determine misalignment between sensor and vehicle body frame; however, misalignment estimation depending on non-holonomic constraint has limitations in high speed environments and there is a lack of observability for roll misalignment.
This paper suggests an online misalignment estimation method under dynamic conditions that violates the non-holonomic constraint. It provides roll, pitch and yaw misalignment angles of IMU mounted on a vehicle, and corresponding sideslip angle of the vehicle at the position of IMU. The misalignment estimator is designed as a linear error state Kalman filter, which takes the results of a strapdown inertial navigation working simultaneously. Computer simulations and real environment experiments with consumer grade GPS and MEMS IMU are performed to demonstrate the performance and reliability of the given method.

KEY WORDS: inertial navigation system, sensor alignment, self-calibration

NOMENCLATURE

$\boldsymbol{x}^{\boldsymbol{i}}$: Vector x in i-frame
$\boldsymbol{p}$: Position
$\boldsymbol{v}$: Velocity
$\boldsymbol{\Psi}$: Attitude in Euler angles (Z-Y-X)
$\boldsymbol{a}$: Acceleration with gravity
$\boldsymbol{f}$: Specific force
$\boldsymbol{\omega}$: Angular rate
$\boldsymbol{\gamma}$: Misalignment angle
$\boldsymbol{\beta}$: Sideslip angle
$\boldsymbol{C}_{\boldsymbol{i}}^{\boldsymbol{k}}$: Transform matrix from i-frame to k-frame
$\boldsymbol{l}_{\boldsymbol{g}}, \boldsymbol{l}_{\boldsymbol{o}}$: GPS/Odometer lever arm
$\boldsymbol{g}$: Gravitational vector
$\mathbf{I_i}, \mathbf{O_i}$: Identity/Zero square matrix in i-dimension
$\boldsymbol{\phi}, \boldsymbol{\theta}, \boldsymbol{\psi}$: Roll, pitch and yaw angles

SUBSCRIPTS

$\boldsymbol{n}$: Local navigation frame
$\boldsymbol{b}$: IMU body frame
$\boldsymbol{v}$: Vehicle body frame
$\mathbf{0}$: Sensor bias
$\boldsymbol{ik}$: Measurement for i-frame with respect to k-frame
$\times$: Cross product matrix

* *Seibum Choi*. e-mail: sbchoi@kaist.ac.kr

1. INTRODUCTION

Land vehicle navigation has become standard equipment on many cars. Navigation systems are based on the global navigation satellite system (GNSS). GNSS provides location and velocity measurements, but has a limitation due to signal obscuration in the operation environment,

such as underpasses or urban areas. The strapdown inertial navigation system (SINS) is broadly used to compensate for position and velocity during GNSS signal outage. SINS with GNSS aiding can fill in signal outages, suppress sensor drift accumulation, and provide attitude information (Abbott and Powell, 1999). Furthermore, through information on vehicle attitude and velocity in the vehicle body frame, the integrated system opens the possibility of its being used as a vehicle dynamics sensor as well as a navigation system.

Several studies have been presented on using SINS to estimate vehicle dynamics parameters. Measurements from GNSS in conjunction with the vehicle dynamics control system have potential benefits for precise velocity estimation during anti-lock braking system actuation (Beiker *et al*., 2006). Based on a global velocity measurement of GNSS, a sideslip estimation including cornering stiffness estimation is also introduced. (Bevly *et al*., 2001). Moreover, GNSS combined with vehicle and tire models, tire force estimation can be performed in nonlinear regions (Daily and Bevly., 2004).

While most common navigation systems use a single antenna, a dual antennae system can widely expand the usage of GNSS in vehicle dynamics. A dual antennae system has the ability to measure the attitude of the vehicle directly, based on the longitudinal force balance, vehicle mass, rolling resistance, and drag coefficient (Bae *et al.*, 2001). The roll dynamics is also identified using a lateral antenna baseline (Ryu *et al.*, 2002). Also, a dual antennae system has the advantage of direct sideslip angle measurement, while IMU based systems require accurate vehicle models for the sideslip angle estimation (Oh and Choi, 2013).

Meanwhile, the methods suggested above can provide acceptable estimation performances with consumer grade GNSS. However, there is a prerequisite that IMU should be accurately aligned with respect to the vehicle. A small misalignment of the IMU can result in an erroneous solution (Syed *et al.*, 2008). To reduce the misalignment errors and improve performance, miscellaneous methods are investigated.

In the case of a vehicle moving on a level surface, a simple complementary filter can directly compute misalignment angles from the Earth's rotation rate and gravity. During the alignment process, it is recommended that the vehicle remains stationary. Additionally, consumer grade MEMS sensors cannot distinguish the Earth's rotation rate from measurement noise, hence the system loses observability of global yaw misalignment (Nebot *et al.*, 1999). When the vehicle is moving, the gravity aided alignment is no longer available due to the translational acceleration. To deal with in-motion alignment, the non-holonomic constraint (NHC) has been adopted as virtual velocity aiding. A system integrated with odometers can provide pitch and yaw misalignments, though the roll misalignment is still unknown (Wu *et al.*, 2009, Chen *et al.*, 2020).

The absence of roll misalignment observability restricts the application of SINS as a vehicle dynamics sensor. Several approaches have been introduced to estimate roll misalignment. When a vehicle travels along straight line on a horizontal plane, the specific force and angular rate reconstructed from the trajectory can be used to determine misalignment angles (Bao *et al.*, 2013). An alternative method has been proposed to estimate misalignment angles in general driving maneuvers rather than a straight line by assuming that only the centripetal force acts on the vehicle in the lateral direction. (Larsson et al., 2017, Zheng et al., 2017).

The methods presented previously are built upon the non-holonomic constraint, which violates the actual vehicle dynamics with lateral motion and the violation is transferred to alignment errors. A different approach based on the single-track model is proposed in order to avoid limitations of the non-holonomic constraint (Marco et al., 2021). The single-track model is widely adopted to approximate the lateral dynamics of vehicle, but it requires accurate prior knowledge of vehicle model parameters, such as cornering stiffness and moment of inertia of vehicle.

This paper suggests an alternative method for in-motion alignment estimation of vehicle mounted SINS, which secures performance under highly dynamic conditions. The suggested method assumes that the vehicle is moving on a planar surface without a suspension motion. The misalignment angles are obtained using an error state Kalman filter from the virtual acceleration, including the rate of the sideslip angle as a pseudo measurement.

The remainder of this paper is organized as follows. Section II presents the formulation of SINS in the local navigation frame. Section III presents the proposed misalignment estimation algorithm. Section IV shows the results of misalignment estimation through simulation and real environment experiments. Finally, section V provides the conclusions.

2. STRAPDOWN INS FORMULATION

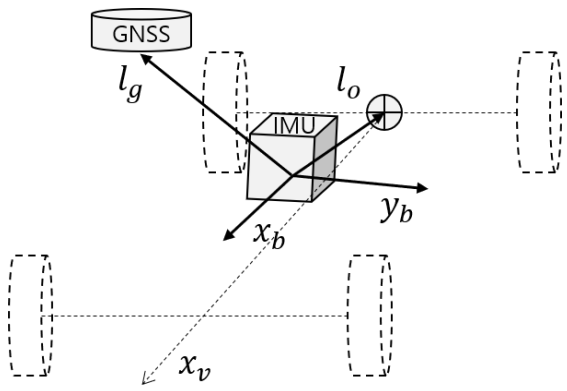

Figure 1. System mounted on vehicle

The system used in this research is briefly illustrated in Figure 1. IMU is mounted on vehicle body in the position of l_o from the center of the rear axle. Note that there are misalignments in installation between the IMU and the vehicle body frame. The GNSS antenna is located on the loop, with lever arm l_g from IMU.
In this section, the mathematical formulation and corresponding error state model of SINS are presented.

2.1. Strapdown System Mechanization

The SINS mechanization can be represented in several frames, e.g., Earth-Centered Earth-Fixed frame, local navigation frame, or vehicle body frame. In this paper, the mechanization equations follow the local navigation frame representation (Titterton *et al.*, 2004).

2.1.1. Attitude Update Equation

The SINS attitude matrix is represented by three Euler angles, ϕ (roll), θ (pitch), and ψ (yaw), with Z-Y-X order of successive rotation from the IMU frame to the local navigation frame.

$$C_b^n = C_\phi C_\theta C_\psi = \begin{bmatrix} c\theta c\psi & -c\phi s\psi + s\phi s\theta c\psi & s\phi s\psi + c\phi s\theta c\psi \\ c\theta s\psi & c\phi c\psi + s\phi s\theta s\psi & -s\phi c\psi + c\phi s\theta s\psi \\ -s\theta & s\phi c\theta & c\phi c\theta \end{bmatrix} \quad (1)$$

Here, *c* and *s* refer to sine and cosine. The time update of C_b^n satisfies the kinematic equation, as follows

$$\dot{C_b^n} = C_b^n \omega_{nb\times}^n \quad (2)$$

$$\omega_\times = \begin{bmatrix} 0 & -\omega_z & \omega_y \\ \omega_z & 0 & -\omega_x \\ -\omega_y & \omega_x & 0 \end{bmatrix} \quad (3)$$

where ω_{nb}^b is the angular rate of the IMU frame with respect to the navigation frame. The operator $\cdot_\times$ denotes a skew-symmetric matrix for a vector, which satisfies the cross product of vectors, $a \times b = a_\times b$.

2.1.2. Velocity and Position Update Equation

Applying general three-dimensional equations of motion on a rotating frame, the derivative of velocity takes the form,

$$f_b^n = C_b^n a^b - g^n \quad (4)$$

$$\dot{v^n} = f_b^n - (2\omega_{ie}^n + \omega_{en}^n) \times v^n \quad (5)$$

where f_b^n is the specific force represented in the local navigation frame, a^b is the acceleration of IMU frame, g^n is the gravity in local navigation frame, ω_{ie}^n is the Earth rotation rate and ω_{en}^n is the transport rate. However, the magnitudes of ω_{ie}^n and ω_{en}^n are in the order of 10^{-6}, while the specific force f has a value on the order of ~ 10. (Hong *et al.*, 2005)
Therefore, by assuming that the rotation rate of the local navigation frame with respect to the inertial frame is negligible, the velocity and position update can be simplified as follows

$$\dot{v^n} = f_b^n \quad (6)$$

$$\dot{p^n} = v^n \quad (7)$$

where v^n and p^n denote the velocity and position in the local navigation frame.
Through a series of inertial measurements, Equations (2), (6) and (7) provide navigation solutions for position, velocity and attitude from the initial state of the SINS. Since the mechanization process has only integration steps, there are two major factors that contribute to increasing the error: one is the sensor bias, the other is the initial alignment. (Dissanayake et al., 2001, Syed et al., 2019) Thus, to suppress the error growth with time integration, an estimation algorithm for both sensor bias and misalignment is required.

2.2. Error State Kalman Filter

In this paper, an error state Kalman filter is used for a loosely-coupled integration of GNSS and SINS (Woodman, 2007). The GNSS measurements, position and velocity, are utilized to correct the SINS solutions introduced in the previous section. The Kalman filter takes position, velocity and attitude as its states. In addition, sensor bias and lever arm estimations are also implemented to compensate for the raw measurements.

2.2.1. Error Propagation

The result of the SINS and GNSS solution can be divided into estimated states and corresponding errors. The error state is defined as the residual between ground truth and estimated state,

$$p^n = \hat{p}^n + \delta p^n \quad (8)$$

$$v^n = \hat{v}^n + \delta v^n \quad (9)$$

$$C_b^n = \delta C_b^n \hat{C}_b^n \quad (10)$$

$$l_g = \hat{l}_g + \delta l_g \quad (11)$$

where δp, δv, δC_b^n and δl_g refer estimation errors in position, velocity, rotation matrix from IMU to local navigation frame and GNSS antenna lever arm. Since the attitude errors are assumed to be small, δC_b^n can be approximated using Euler angles, $\delta\phi, \delta\theta$ and $\delta\psi$,

$$\delta C_b^n \approx \begin{bmatrix} 1 & -\delta\psi & \delta\theta \\ \delta\psi & 1 & -\delta\phi \\ -\delta\theta & \delta\phi & 1 \end{bmatrix} = [\mathbf{I} + \Psi_\times] \quad (12)$$

$$C_b^n \approx [\mathbf{I} + \Psi_\times]\hat{C}_b^n \quad (13)$$

where Ψ is the attitude error vector $\Psi = [\delta\phi \quad \delta\theta \quad \delta\psi]$. The measurements from accelerometer and gyroscope are augmented into the error state to eliminate the effect of measurement biases. The sensor biases are constants or very slow varying quantities compared with other state variables, hence the acceleration and angular rate acting on IMU frame become

$$a^b = \hat{a}^b + a_0^b \tag{14}$$
$$\omega_{nb}^b = \hat{\omega}_{nb}^b + \omega_0^b \tag{15}$$

where $\hat{a}^b$ and $\hat{\omega}_{ib}^b$ are the compensated acceleration and angular rate, and a_0^b and ω_0^b are sensor biases. Note that equation (15) represents the angular rate of IMU frame *b* with respect to the local navigation frame *n*, since the Earth rotation rate and transport rate are negligible.
Substituting equations (8)-(15) into the mechanization equations (2)-(7), the error state model of strapdown navigation can be derived. Assuming the errors have small values, the error state model can be linearized as

$$\delta\dot{p}^n = \delta v^n \tag{16}$$
$$\delta\dot{v}^n = f_{b\times}^n \Psi + C_b^n \delta a_0^b \tag{17}$$

The error propagation of attitude error uses the Euler angle vector Ψ, rather than the rotation matrix δC_b^n. From the definition of δC_b^n and $\delta\dot{C}_b^n$, the time derivative of rotational error in matrix form is

$$\begin{aligned}\delta\dot{C}_b^n &= \dot{C}_b^n \hat{C}_n^b + C_b^n \dot{\hat{C}}_n^b \\ &= C_b^n \omega_{nb\times}^b \hat{C}_n^b + C_b^n \hat{C}_n^b \hat{\omega}_{bn\times}^n\end{aligned} \tag{18}$$

where both $\omega_{\mathrm{nb}}^{\mathrm{b}}$ and $\hat{\omega}_{\mathrm{bn}}^{\mathrm{n}}$ are the angular rate of IMU, but represented in different perspectives. Applying inverse rotation matrices and substituting δC_b^n with Ψ (12),

$$\begin{aligned}C_n^b \delta\dot{C}_b^n \hat{C}_b^n &= \omega_{nb\times}^b + \hat{C}_n^b \hat{\omega}_{bn\times}^n \hat{C}_b^n \\ &= \omega_{nb\times}^b - \hat{\omega}_{nb\times}^b \\ &\approx C_n^b \Psi_\times C_b^n = \left[C_n^b \Psi\right]_\times\end{aligned} \tag{19}$$

Then, the vector form of attitude error propagation can be written as follows

$$\Psi \approx C_b^n(\omega_{nb}^b - \hat{\omega}_{nb}^b) = C_b^n \omega_0^b \tag{20}$$

With the error state model (14)-(20), the corresponding system dynamics in discrete-time system is

$$\delta x = \left[\delta p^n \quad \delta v^n \quad \Psi \quad a_0^b \quad w_0^b \quad \delta l_g\right] \tag{21}$$
$$\delta x_{k+1} = \Phi \delta x_k + G w_k \tag{22}$$

where w_k is unknown input noise.

Taking derivative of equations (16)-(20) with respect to the error state δx, corresponding state transition matrix *F* and discrete-time transition matrix Φ can be calculated as follows

$$F = \begin{bmatrix} \mathbf{0_3} & \mathbf{I_3} & \mathbf{0_3} & \mathbf{0_3} & \mathbf{0_3} & \mathbf{0_3} \\ \mathbf{0_3} & \mathbf{0_3} & f_{b\times}^n & C_b^n & \mathbf{0_3} & \mathbf{0_3} \\ \mathbf{0_3} & \mathbf{0_3} & \mathbf{0_3} & \mathbf{0_3} & C_b^n & \mathbf{0_3} \\ \mathbf{0_3} & \mathbf{0_3} & \mathbf{0_3} & \mathbf{0_3} & \mathbf{0_3} & \mathbf{0_3} \\ \mathbf{0_3} & \mathbf{0_3} & \mathbf{0_3} & \mathbf{0_3} & \mathbf{0_3} & \mathbf{0_3} \\ \mathbf{0_3} & \mathbf{0_3} & \mathbf{0_3} & \mathbf{0_3} & \mathbf{0_3} & \mathbf{0_3} \end{bmatrix} \tag{23}$$
$$\Phi = exp(F) \approx I + F\Delta t \tag{24}$$

where $\mathbf{0_3}$ refers 3 by 3 null matrix and $\mathbf{I_3}$ refers identity matrix.
The measurement noise of an inertial sensor is typically defined with a combination of white noise and random walk (Quinchia *et al.*, 2013). Then input noise covariance matrix G can be simplified as follows

$$G = \begin{bmatrix} \mathbf{0_3} & \mathbf{0_3} & \mathbf{0_3} & \mathbf{0_3} \\ C_b^n & \mathbf{0_3} & \mathbf{0_3} & \mathbf{0_3} \\ \mathbf{0_3} & -C_b^n & \mathbf{0_3} & \mathbf{0_3} \\ \mathbf{0_3} & \mathbf{0_3} & \mathbf{I_3} & \mathbf{0_3} \\ \mathbf{0_3} & \mathbf{0_3} & \mathbf{0_3} & \mathbf{I_3} \\ \mathbf{0_3} & \mathbf{0_3} & \mathbf{0_3} & \mathbf{0_3} \end{bmatrix} \tag{25}$$

Applying $Q_d = E[w_k w_k^T]$, the covariance of process noise Q is obtained in terms of IMU characteristics,

$$\begin{aligned}Q_k &= G \begin{bmatrix} \sigma_{acc,std}^2 & \mathbf{0_3} & \mathbf{0_3} & \mathbf{0_3} \\ \mathbf{0_3} & \sigma_{gyr,std}^2 & \mathbf{0_3} & \mathbf{0_3} \\ \mathbf{0_3} & \mathbf{0_3} & \sigma_{acc,rw}^2 & \mathbf{0_3} \\ \mathbf{0_3} & \mathbf{0_3} & \mathbf{0_3} & \sigma_{gyr,rw}^2 \end{bmatrix} G^T \Delta t \\ &= G Q_d G^T \Delta t\end{aligned} \tag{26}$$

where σ_{std} means the standard deviation of white noise and σ_{rw} is the random walk in discrete-time. Δt is the sampling time between IMU measurements.

2.2.2. Measurement Model
Considering a general scenario of mounting GNSS and SINS on a vehicle, a lever arm l_g, between the IMU and the GNSS antenna, exists in most cases. This lever arm directly affects the position measurement, and also influences on the velocity measurement, depending on the angular rates of motion. Then, the difference between the SINS solution and the GNSS measurement can be represented with lever arm l_g

$$z = \begin{bmatrix} p_{gnss}^n \\ v_{gnss}^n \end{bmatrix} \tag{27}$$

$$\hat{z} = \begin{bmatrix} p^n + C_b^n l_g \\ v^n + C_b^n \omega_{bn\times}^n l_g \end{bmatrix} \quad (28)$$

where z is GNSS position and velocity measurement from the receiver, $\hat{\mathrm{z}}$ is the estimated measurement with antenna lever arm compensation. The error of estimated position and velocity becomes

$$\delta z = \begin{bmatrix} p^n + C_b^n l_g - p_{gnss} \\ v^n + C_b^n \omega_{bn\times}^n l_g - v_{gnss} \end{bmatrix} \quad (29)$$

When all of the error states δx have exact values, the difference between $\hat{z}$ and z, is expected to be zero. Thus, δz becomes the measurement error itself.
Substituting equations (8)-(15) into (29) and taking the derivative of the measurement error δz, with respect to the state vector δx, the measurement matrix H becomes,

$$H = \quad (30)$$
$$\begin{bmatrix} \mathrm{I}_3 & \mathrm{O}_3 & \hat{C}_b^n \hat{l}_{g\times} \hat{C}_b^{nT} & \mathrm{O}_3 & \mathrm{O}_3 & \hat{C}_b^n \\ \mathrm{O}_3 & \mathrm{I}_3 & -\left[\hat{C}_b^n (\hat{l}_g \times \hat{\omega}_{bn}^n)\right]_\times & \mathrm{O}_3 & -\hat{C}_b^n \hat{l}_{g\times} & \hat{C}_b^n \hat{\omega}_{bn\times}^n \end{bmatrix}$$

while the high order terms are neglected under the small error assumption.
The integration process of SINS and GNSS is slightly modified from the standard Kalman filtering sequence. Since the update rate of GNSS is much slower than that of the IMU, the correction step is only performed when GNSS provides measurements, while several prediction steps are processed using IMU measurements, during the GNSS interval.

Table 1. Update sequence for multi rate measurements.

IMU measurement	$\hat{x}_k^- = \Phi \hat{x}_{k-1}^-$ $P_k^- = \Phi P_{k-1}^+ \Phi^T + G Q_d G^T$
GNSS measurement	$K_k = P_k^- H_k^T (H_k P_k^- H_k^T + R_k)^{-1}$ $\hat{x}_k^+ = \hat{x}_k^- + K_k (z_k - H_k \hat{x}_k^-)$ $P_k^+ = (\mathbf{I} - K_k H_k) P_k^- (\mathbf{I} - K_k H_k) + K_k R_k K_k^T$

3. MISALIGNMENT ESTIMATION

The position, velocity and attitude estimations from SINS are resolved in the IMU coordinate, not in the vehicle body frame. In this section, an estimation method for the misalignment angles between the IMU and the vehicle body frame is introduced.
In this section, two models are introduced and fused with SINS solutions via Kalman filtering, in which the state is three misalignment angles γ, which satisfies $C_b^v \approx [\mathbf{I} + \gamma_\times]\hat{C}_b^v$. It is assumed that misalignment γ has small values, with proper coarse initial alignment. In this paper, the fast-optimal attitude matrix (FOAM) method is implemented to initialize coarse alignments (Markley, 1993).

3.1. Non-holonomic Constraint Model

In the case of land vehicles, the motion on a surface is restricted by non-holonomic constraints. When the sideslip angle of vehicle is negligible, the axle without steering should not move sideways, and all wheels should maintain contact with the ground. Under these constraints, the virtual measurement of the velocity of a rear axle can be derived as

$$v_{nhc}^v = C_b^v v^b + C_b^v \omega_{nb}^b \times l_o \approx \begin{bmatrix} v_{odo} \\ 0 \\ 0 \end{bmatrix} \quad (31)$$

where l_o stands for the distance vector between the IMU and the rear axle center, which is unknown for most cases. Since non-holonomic constraint is regulating the motion of the rear axle, it is required to estimate the odometry lever arm as well as the misalignment angles simultaneously. Hence, in-motion alignment algorithms based on NHC require additional velocity measurement for lever arm estimation such as an odometer (Xue et al., 2017).
However, when using NHC to estimate misalignment angles, there is a lack of observability because the Euler angle ϕ is irrelevant to the measurements (Wu *et al.*, 2012, Lee *et al.*, 2012). Expanding the rotational matrices with the Euler angle, Equation (31) becomes

$$C_v^b v_{odo} = \begin{bmatrix} \cos\theta_b^v \cos\psi_b^v \\ \cos\theta_b^v \sin\psi_b^v \\ -\sin\theta_b^v \end{bmatrix} v_{odo} = v^b + \omega_{nb}^b \times l_o \quad (32)$$

Thus, roll misalignment ϕ_b^v is unobservable regardless of the motion of vehicle.
In the same manner as in chapter 2, Equation (31) can be rewritten for small errors

$$\begin{aligned} \delta v_{nhc}^v &= [\mathbf{I} - \gamma_\times] C_b^v v^b + [\mathbf{I} - \gamma_\times] C_b^v \omega_{nb}^b \times (l_o + \delta l_o) \\ &= v_{nhc}^v - H_{nhc} \delta x \end{aligned} \quad (33)$$
$$H_{nhc} = \begin{bmatrix} \hat{C}_b^v v^b \hat{C}_b^{vT} - \hat{l}_{o\times} \hat{C}_b^v \omega_{nb}^b \hat{C}_b^{vT} & \hat{C}_b^v \omega_{nb}^b \hat{C}_b^{vT} \end{bmatrix} \quad (34)$$

where γ is the misalignment rotation matrix of the IMU with respect to the vehicle body frame, $\gamma = [\phi_b^v, \theta_b^v, \psi_b^v]$, δl_o is an odometer lever arm vector in the vehicle body frame and δx is the error state for misalignment estimation, $\delta x = [\gamma \quad \delta l_o]$.

3.2. Planar Dynamics Model

The sufficient condition of the NHC model is only valid for cars moving at low speed without tire slip. Thus, to maintain the estimation performance in high speed or high acceleration scenarios, a new approach is required. Without considering the suspension movement, the vehicle motion on a surface can be represented as the sum of the translation on a plane and the rotation about the axis perpendicular to the plane.

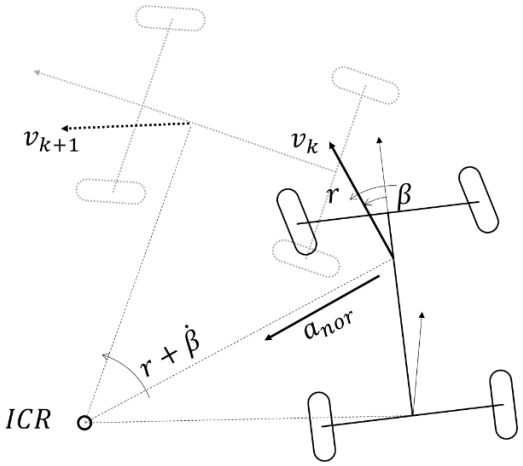

Figure 2. Motion of vehicle on surface

In a short period of motion, the centrifugal force, toward the instantaneous center of rotation, can be represented with the angular rate and magnitude of the velocity. As shown in Figure 2, the direction change of the velocity contains the slip rate $\dot{\beta}$, so the centrifugal force also has a relationship with $\dot{\beta}$. This can be seen in Figure 3, where the black line represents the centrifugal force from the computer simulation, and the red and blue lines represent the centrifugal forces reconstructed from the motion with or without considering the slip rate.

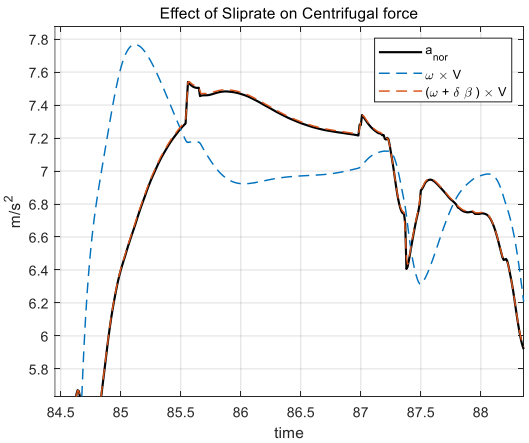

Figure 3. Planar acceleration reconstructed from motion of vehicle with sideslip

A surface can be treated as a plane locally during the short-term motion. Then, the specific force aligned with the direction of the velocity in the vehicle body frame can be approximated as follows

$$\dot{v}_{tan} = \frac{v^n}{|v^n|} \cdot f_b^n \approx |\dot{v}^n| \tag{35}$$

and the specific force toward the instantaneous center of rotation is given by

$$\dot{v}_{nor} = -\dot{\hat{\beta}}|v^n| \tag{36}$$

where $\hat{\beta}$ is estimated sideslip angle at the point of IMU, defined as $\hat{\beta} = \tan^{-1}(\frac{\hat{v}_y^v}{\hat{v}_x^v})$ with the velocity in vehicle body frame $\hat{v}^v = \hat{C}_b^v v^b$. Similarly, the angular rate resolved in the planar coordinate becomes

$$\omega_{binor} = |\omega^n| \tag{37}$$

ω_{binor} only has the value along the binormal axis, since it is assumed that the vehicle lies on a plane locally. However, the derivative of the velocity in the vehicle body frame is

$$\dot{v^v} = C_b^v\left(a^b - C_n^b g^n - \omega_{nb}^b \times v^b\right) \tag{38}$$

Now, based on above assumptions (35), (36) and (37), the errors on virtual measurements of specific force and angular rate on vehicle body frame is given by

$$\delta\dot{v^v} = [\mathbf{I} - \gamma_\times]\hat{C}_b^v\left(a^b - C_n^b g^n - \omega_{nb}^b \times v^b\right) - \hat{\beta}_\times \begin{bmatrix} |\dot{v^n}| \\ \dot{\hat{\beta}}|v^n| \\ 0 \end{bmatrix} \tag{39}$$

$$\delta\omega^v \approx [\mathbf{I} - \gamma_\times]\hat{C}_b^v\omega_{nb}^b - \begin{bmatrix} 0 \\ 0 \\ |\omega| \end{bmatrix} \tag{40}$$

where $\hat{\beta}_\times$ is the transform matrix, rotating $\hat{\beta}$ about the z axis of the vehicle body frame.
The corresponding matrix derivative of (39) and (40), with respect to the misalignment γ, is as follows

$$H_{planar} = \begin{bmatrix} \left[\hat{C}_b^v\left(a^b - C_n^b g^n - \omega_{nb}^b \times v^b\right)\right]_\times \\ \hat{C}_b^v\omega_{nb\times}^b\hat{C}_b^{vT} \end{bmatrix}^T \tag{41}$$

With the virtual measurements (33) and (39), a linear Kalman filter is formulated to estimate the misalignment angles. The misalignment KF introduced in the previous section has 6 state variables, 3 misalignment angles γ and odometer lever arm error δl_o. However, applying the planar dynamics model, odometry lever arm error δl_o is

fully isolated from the estimation process because the measurement model (41), does not contain additional states more than misalignment angles γ.
The misalignment KF is updated when there is a SINS update with new IMU measurements. The solution of SINS is basically the result of the integrations. Thus, the magnitude of states does not drastically change. However, when the measurement update occurs with new GNSS measurement, the estimated state changes significantly over a short period of time. This gap between two successive states results in an irrational value of slip rate $\dot{\hat{\beta}}$. In order to handle the potential instability, the misalignment estimator re-initializes its states when the solution of SINS has been updated from the GNSS measurement.

4. SIMULATION AND EXPERIMENT RESULTS

In this section, simulation and real vehicle test are performed to evaluate the estimation performance of the suggested algorithm.

4.1. Simulation Results

Before moving on to the field test, a simulation based on CarSim and MATLAB was performed to ensure the stability and performance of the suggested algorithm. GNSS measurements are replaced with local positions and the velocity in the reference frame; proper Gaussian noise is added to emulate real GNSS measurements.
A low cost IMU has an output error that is a combination of bias, sensitivity shift and noise. In this simulation, a sensor error model considering bias and white noise is implemented. The parameters of the sensor noise follow those of typical consumer grade IMU (Gebre-Egziabher, 2004).

Table 2. Simulated sensor geometry

Antenna lever arm	X: 0, Y: 0.4, Z: 0.2	m
Odometer lever arm	X: -1.8, Y: 0, Z: 0	m
IMU Misalignment	Roll: 0.1, Pitch: -0.1, Yaw: 0.2	rad

Table 3. Simulated noise parameters

Position accuracy	2.55 (3.0 CEP)		m
Velocity accuracy	0.2		m/s
Accelerometer	Noise Bias	0.1 [0.2, -0.1, 0.2]	m/s^2
Gyro	Noise Bias	0.01 [-0.01, 0.008, 0.004]	rad/s

In order to show the differences between NHC and the suggested method, a closed loop track is chosen so as to maintain harsh driving during the entire simulation. Although the acceleration is bounded to a value under 0.7g, the sideslip occurs on the rear axle, which violates NHC.

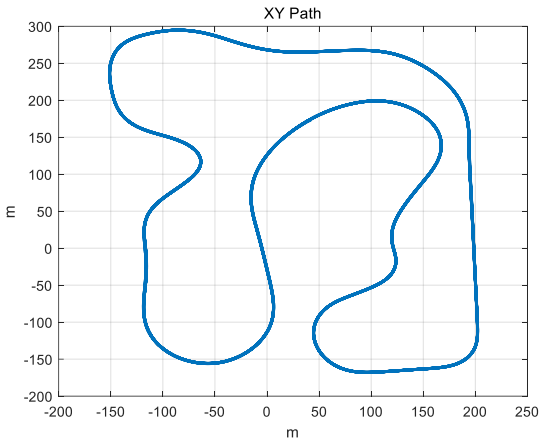

Figure 4. Simulation track layout

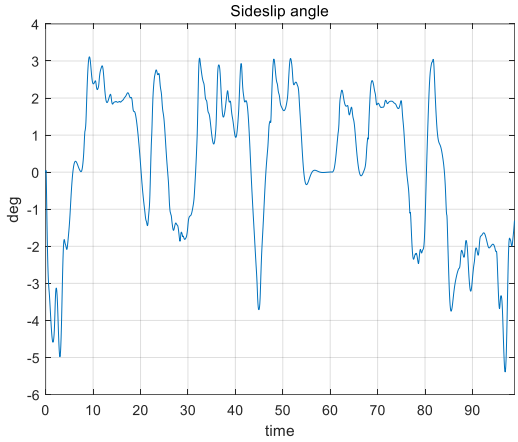

Figure 5. Slip on rear axle center

The simulation results of the misalignment estimation are illustrated in Figures 6-8. Both the NHC and the suggested methods are implemented using the same data. The NHC method converges to wrong values of yaw and pitch misalignment, whereas roll misalignment is not observable, as described in the previous section.
The suggested method yields enhanced performance compared with the conventional NHC method. The roll misalignment, now can be observed, and estimation errors of misalignment angles are reduced under harsh maneuvers.
Additionally, the proposed method can operate with roll and pitch angles when the vehicle stops, whereas NHC methods totally lose their observability when there is no motion. As can be seen in Equation (39), the virtual measurement $\delta\dot{v}^v$ contains gravitational components, even though $|\dot{v^n}|$ and $|v^n|$ are zero.

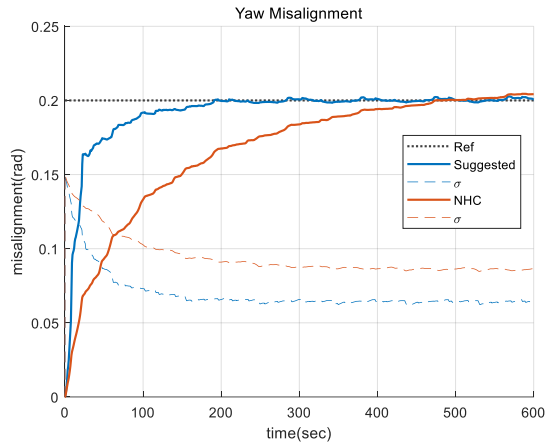

Figure 6. Yaw misalignment estimation (simulation)

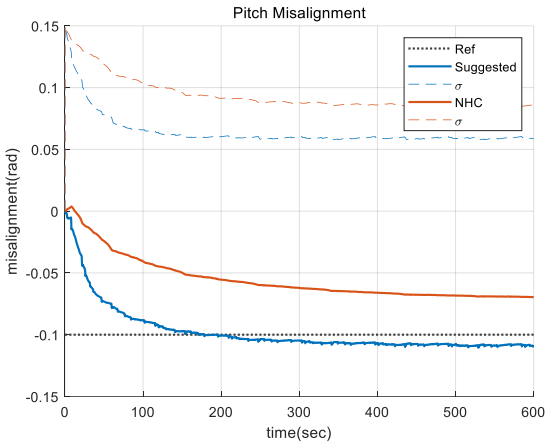

Figure 7. Pitch misalignment estimation (simulation)

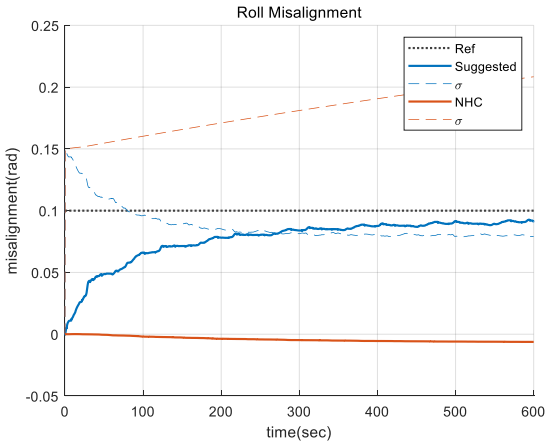

Figure 8. Roll misalignment estimation (simulation)

4.2. Experimental Results

A field test was performed to verify the estimation performance under real conditions with uncertainties. Oxts RT3100 is equipped in the test vehicle as a reference measurement. A Ublox M8U GNSS receiver and TDK ICM-42605 IMU are used in the test. The update rate of the IMU is set to 200Hz, while the update rate of the GNSS receiver is set to 10Hz.

In order to align the IMU along the reference sensor and add artificial misalignment, a high-precision rotational stage is used. The true misalignment angles used in the experimental setup are shown in Table 4.

Table 4. Misalignment angles in tests

	Yaw(rad)	Pitch(rad)	Roll(rad)
Vehicle-RT	0.02	-0.0471	0.0157
RT-IMU	0.1745	0	0
Vehicle-IMU	0.1945	-0.0471	0.0157

The misalignment between the vehicle and RT3100 is obtained using fine calibration on a near-level surface. The rotational stage is set to additional 10 degrees in yaw angle(0.1745 in radian) for target IMU.

Figure 9. Sensors with rotational stage used in test

The experiment was performed at the Taebaek Speedway in S. Korea, which is a small race track with 2.5km length.

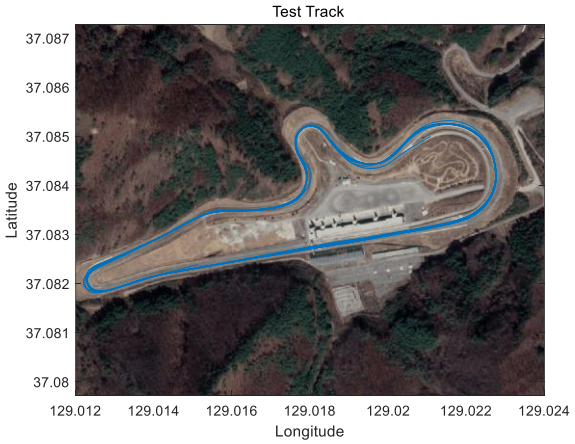

Figure 10. Test track layout (Taebaek Speedway)

Note that the experimental data have much longer lengths than those of the simulated data used in the previous section. Due to the surrounding environment, there is a shaded area in the route, where GNSS receiver cannot lock onto enough satellite for a position fix. Thus, error covariances of measurement have higher values than those of simulated data, which means that the system requires a longer time for stabilization.

Figures 11-13 present the results of misalignment angle estimation, comparing the NHC and suggested methods. As was seen before in the simulation results, the suggested model gives better performance for yaw and pitch estimation.

Figure 13 shows the roll misalignment estimation. Both the suggested and NHC methods have estimation errors, but the state covariance of the suggested method tends to find a steady state value, whereas that of the NHC method floats around the initial value.

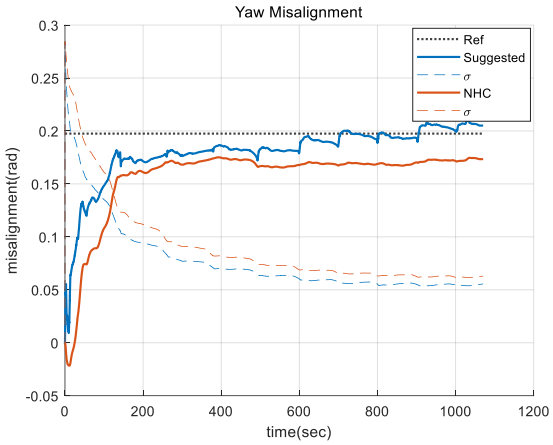

Figure 11. Yaw misalignment estimation (real vehicle)

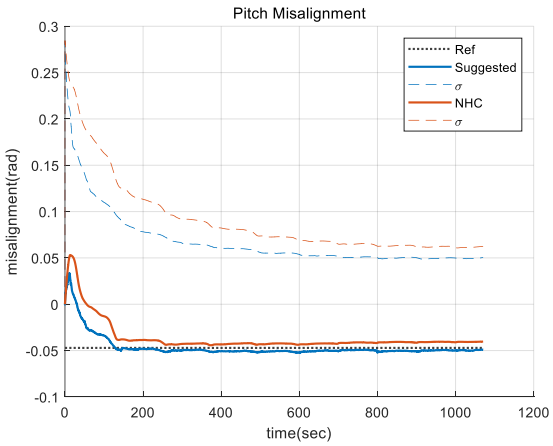

Figure 12. Pitch misalignment estimation (real vehicle)

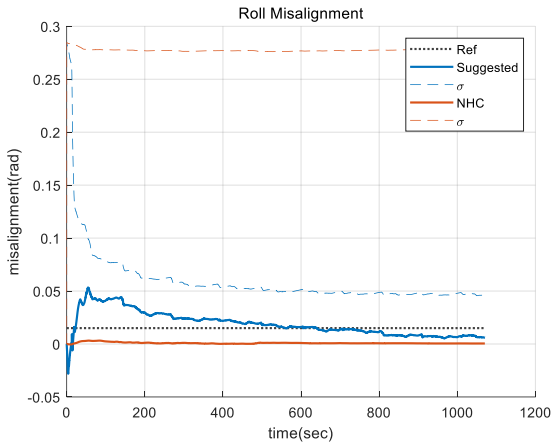

Figure 13. Roll misalignment estimation (real vehicle)

Even though the test vehicle generates severe suspension motion during the experiment maneuvers, which violates the assumption presented in Section 3, the proposed alignment method provides acceptable accuracy under highly dynamic conditions.

However, the initial response of the experimental results differs from the simulated results. In the simulation, each misalignment angle tends to converge from the beginning of estimation, while the experimental results show some fluctuations. These fluctuations are considered to be caused by initial errors of the SINS attitude. Because the misalignment estimator uses attitude to construct virtual measurements in vehicle body frame, the global attitude error can directly affect the performance of misalignment angle estimation.

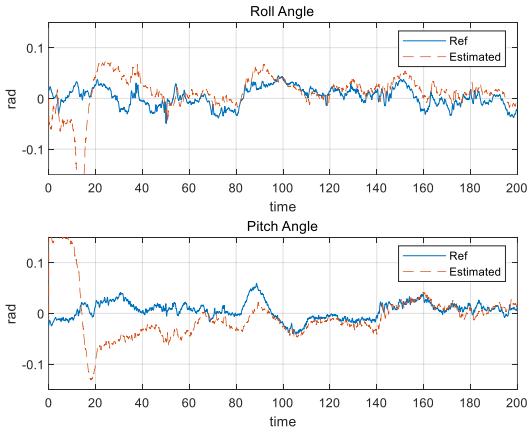

Figure 14. Vehicle roll and pitch angle.

Corresponding attitude estimation results for vehicle roll and pitch angles are presented in Figure 14. Since the suggested method estimates sensor bias as well as position, velocity, and attitude simultaneously, the error seems fluctuating within stabilization period, while the error decreases as other states, such as sensor bias,

converge. After misalignment estimation is settled, compensated attitude also follows the reference, with RMSE less than 1.5° .

As demonstrated in these results, the online misalignment estimation based on the planar dynamics model shows improved performance compared to the non-holonomic constraint method, regardless of the motion of the target system.

5. CONCLUSION

This paper has shown the feasibility of a novel mis-alignment estimation method for SINS on land vehicles using IMU and GNSS integration. The proposed method uses simple planar dynamics constraints to obtain IMU to vehicle body frame misalignment. As mentioned earlier, the proposed method can estimate misalignment angles without non-holonomic restrictions, including roll observation.

A real environment experiment on a race track was performed to demonstrate the estimation performance under dynamic maneuvers with consumer grade sensors. The results show an improvement of the misalignment estimation compared with conventional approaches regardless of motion constraints or prior knowledge of vehicle model parameters.

ACKNOWLEDGEMENTS– This work was supported by a Korea Evaluation Institute of Industrial Technology(KEIT), grant funded by the Korean government(MOTIE)(20005609, Active Suspension System for Improvement over 5% Ride and Handling Performance using Road Surface and Road Shape); the BK21+ program through the NRF funded by the Ministry of Education of Korea; and a grant(20TLRP-C152478-02) from the Transportation & Logistics Research Program funded by the Ministry of Land, Infrastructure and Transport(MOLIT) of the Korean government and the Korea Agency for Infrastructure Technology Advancement(KAIA).

REFERENCES

Abbott, E. and Powell, D. (1999). Land-Vehicle Navigation Using GPS. Proceedings of the IEEE 87, 1, 145-162.

Bae, H. S., Ryu, J., and Gerdes, J. C. (2001). Road grade and vehicle parameter estimation for longitudinal control using GPS. In Proceedings of the IEEE Conference on Intelligent Transportation Systems 25-29.

Bao, Z., Lu, G., Wang, Y., and Tian, D. (2013) A calibration method for misalignment angle of vehicle-mounted IMU. Procedia-Social and Behavioral Sciences 96, 1853-1860.

Beiker, S.A., Gaubatz, K.H., Gerdes, J.C. and Rock, K.L. (2006) GPS Augmented Vehicle Dynamics Control. Journal of Passenger Car: Mechanical Systems Journal 115, 6, 1174-1182.

Bevly, D.M., Sheridan, R. and Gerdes, J.C (2001) Integrating INS Sensors with GPS Velocity Measurements for Continuous Estimation of Vehicle Sideslip and Tire Cornering Stiffness. Proceedings of the 2001 American Control Conference 25-30.

Chen, Q., Zhang, Q., and Niu, X. (2020). Estimate the Pitch and Heading Mounting Angles of the IMU for Land Vehicular GNSS/INS Integrated System. IEEE Transactions on Intelligent Transportation Systems.

Daily, R. and Bevly, D.M. (2004) The Use of GPS for Vehicle Stability Control Systems. IEEE Transactions on Industrial Electronics 51, 2, 270-277.

Dissanayake, G., Sukkarieh, S., Nebot, E., & Durrant-Whyte, H. (2001). The aiding of a low-cost strapdown inertial measurement unit using vehicle model constraints for land vehicle applications. IEEE transactions on robotics and automation, 17, 5, 731-747.

Gebre-Egziabher, D., Hayward, R. C., and Powell, J. D. (2004). Design of Multi-sensor Attitude Determination Systems. IEEE Transactions on aerospace and electronic systems, 40, 2, 627-649.

Hong, S., Lee, M. H., Chun, H. H., Kwon, S. H., and Speyer, J. L. (2005). Observability of Error States in GPS/INS Integration. IEEE Transactions on Vehicular Technology, 54, 2, 731-743.

Lee, M. H., Park, W. C., Lee, K. S., Hong, S., Park, H. G., Chun, H. H., and Harashima, F. (2012). Observability Analysis Techniques on Inertial Navigation Systems. Journal of System Design and Dynamics, 6, 1, 28-44.

Markley, F. L. (1993). Attitude Determination Using Vector Observations: A Fast Optimal Matrix Algorithm. Journal of the Astronautical Sciences 41, 2, 261-281.

Nebot, E., and Durrant-Whyte, H. (1999). Initial Calibration and Alignment of Low-cost Inertial Navigation Units for Land Vehicle Applications. Journal of Robotic Systems 16, 2, 81-92.

Oh, J. and Choi S.B., (2013) Dynamic Sensor Zeroing Algorithm of 6D IMU Mounted on Ground Vehicles.

International Journal of Automotive Technology 14, 2, 221-231

Rodrigo Marco, V., Kalkkuhl, J., Raisch, J., and Seel, T. (2021). A Novel IMU Extrinsic Calibration Method for Mass Production Land Vehicles. Sensors, 21(1), 7.

Ryu, J., Rossetter, E. J., and Gerdes, J. C. (2002). Vehicle Sideslip and Roll Parameter Estimation Using GPS. In Proceedings of the AVEC International Symposium on Advanced Vehicle Control 373-380.

Syed, Z. F., Aggarwal, P., Niu, X., and El-Sheimy, N. (2008). Civilian Vehicle Navigation: Required Alignment of the Inertial Sensors for Acceptable Navigation Accuracies. IEEE Transactions on Vehicular Technology 57, 6, 3402-3412.

Titterton, D., Weston, J. L., and Weston, J. (2004). Strapdown Inertial Navigation Technology 2nd Edn. IET.

Woodman O.J. (2007) An Introduction To Inertial Navigation. University of Cambridge, Computer Laboratory Technical Report. UCAM-CL-TR-696

Wu, Y., Wu, M., Hu, X., and Hu, D. (2009). Self-calibration for Land Navigation Using Inertial Sensors and Odometer: Observability Analysis. In AIAA Guidance, Navigation, and Control Conference 5970.

Wu, Y., Zhang, H., Wu, M., Hu, X., and Hu, D. (2012). Observability of Strapdown INS Alignment: A Global Perspective. IEEE Transactions on Aerospace and Electronic Systems 48, 1, 78-102.

Xue, H., Guo, X., Zhou, Z., and Wang, K. (2017). In-motion Alignment Algorithm for Vehicle Carried SINS Based on Odometer Aiding. Journal of Navigation, 70(6), 1349-1366.

Zheng, Y., Shokouhi, N., Sathyanarayana, A., and Hansen, J. (2017). Free-positioned smartphone sensing for vehicle dynamics estimation SAE Technical Paper No. 2017-01-0072.